Supersonic Turbulent Boundary Layer Subjected to Adverse Pressure Gradients

P. J. WALTRUP* AND J. A. SCHETZ†
Virginia Polytechnic Institute and State University, Blacksburg, Va.

A set of experimental data is presented for a supersonic, two-dimensional turbulent boundary-layer growing along a flat wind-tunnel test section wall while subjected to a systematic variation of three adverse pressure gradients starting from the same initial conditions. The data are for a nearly adiabatic wall with an initial Mach number and Reynold's number per foot of 2.36 and 11.55×10^6, respectively. Detailed profiles of pitot and static pressure, total temperature, mass flow, and turbulence intensity at four axial stations are presented along with direct measurements of wall shear. It is found that profile shapes are affected more by the magnitude than the character of the pressure gradient except very near the wall. Wall shear is found to increase with distance in the pressure gradient with this increase being a function of both the magnitude and character of the pressure gradient. The turbulence intensity is found to monotonically decrease with vertical distance in the zero pressure gradient region, whereas that in the adverse pressure gradient region increases between the wall and the middle of the boundary layer and then decreases to a relatively low freestream value. Comparison of the data with an "exact" numerical calculation based on an eddy viscosity approach indicates good agreement between profile shapes, but predicted values of wall shear are 8% to 20% low.

Nomenclature

h	= enthalpy
L	= characteristic length
M	= Mach number
P	= pressure
T	= temperature
U	= velocity $= u + u'$
u'	= fluctuating component of velocity
U_τ	= friction velocity $\equiv [\tau_w/\rho_w]^{1/2}$
$(\overline{u'^2}/U_\tau)^{1/2}$	= turbulence intensity
X	= axial distance
Y	= normal distance
η	= transformed normal coordinate
δ	= boundary-layer thickness
ρ	= density
τ	= shear stress

Subscripts

e	= edge condition
o	= tunnel stagnation condition
t_1	= stagnation condition in front of normal shock
w	= wall condition
aw	= adiabatic wall condition

Introduction

THE turbulent boundary layer is one of the most common phenomena in all of fluid dynamics. Consequently, extensive studies of both an analytical and experimental character have been presented which date back more than half a century. Nonetheless, our basic understanding of turbulent shear flows remains rather crude, and the "successful" analytical procedures are all based on heuristic models which commonly ignore the turbulence and seek only to reproduce experimental observations of the time-averaged mean flowfield. Even these successful procedures are speculative in that insufficient data to completely define the mean or turbulent flowfield have been generated. In this respect, workers in the incompressible[1,2] and compressible[3] turbulent boundary-layer fields met recently to assess the relative merits of the various analytical procedures in comparison with experimental data. Two important observations relative to the available data can be made as a result of these meetings: 1) There have been no systematic studies of the effects of various types of pressure gradients on the development of turbulent boundary layers starting from fixed initial conditions. This is true with respect to both the magnitude ($\Delta P/L$) and character (local dP/dX vs "X") of the pressure gradient; 2) Only rarely are both the turbulent properties and mean motion reported or sufficient measurements taken to completely define the mean flowfield (pitot and static pressure, total temperature, turbulence intensity, heat transfer, and wall shear).

Table 1 of Ref. 4 provides a useful, although not exhaustive, consensus of the available experimental data for compressible turbulent boundary layers with and without pressure gradients. Two recent papers (Refs. 5 and 6) are added here for completeness. From this survey one can see that there have not been systematic studies of the effects of many of the important flow parameters where sufficient measurements have been made to completely define the flow, and that reliable data in the literature for supersonic turbulent boundary layers in pressure gradients are generally sparse, especially for adverse pressure gradients.

On the basis of the above considerations, the present experimental program was undertaken aimed at obtaining accurate measurements which completely define the mean flow characteristics and turbulence intensity of a compressible turbulent boundary layer systematically subjected to a series of adverse pressure gradients starting from the same initial conditions. Three different pressure gradients were generated. When taken together, they represent a systematic variation of both the magnitude and character of the pressure gradient. In addition, they have been designed so as to include the three types of adverse pressure gradients one is likely to encounter, i.e. 1)

Presented as Paper 72-311 at the AIAA 7th Thermophysics Conference, San Antonio, Texas, April 10–12, 1972; submitted March 3, 1972; revision received August 18, 1972. This work was supported by the National Science Foundation under Grant NSF-GK20379.

Index category: Boundary Layers and Convective Heat Transfer-Turbulent.

* Current Post-Doctoral Research Fellow, Johns Hopkins University, Applied Physics Laboratory, Silver Spring, Md. Associate Member AIAA.

† Professor and Chairman, Aerospace and Ocean Engineering Department. Associate Fellow AIAA.

$d/dX(dP/dX) > 0$, 2) $d/dX(dP/dX) < 0$, and 3) $d/dX(dP/dX) \cong 0$. Profile measurements were made at four axial stations including the "initial" station. The measurements consisted of: 1) pitot pressure distributions, 2) cone-static pressure measurements, 3) total temperature profiles, 4) hot wire traverses at the initial and final stations, and 5) direct skin-friction measurements on the wall at the last three stations. In addition, 1μ sec spark schlieren photographs were taken from each flowfield.

Besides the accumulation of much needed data from the above experiments, an analytic effort was undertaken to further define the accuracy and the limits of applicability of current analytical methods for the calculation of turbulent boundary layers. Since the purpose here was not to develop a new sophisticated analytical treatment of the boundary-layer equations, an existing numerical program developed by Miner, Anderson, and Lewis[7] was selected as typical of the best available and was used for the comparison.

Experimental Apparatus and Procedure

Wind Tunnel

The tests were conducted in the Virginia Polytechnic Institute and State University 9×9 in. supersonic blowdown wind tunnel. A freestream Mach number of 2.36 with a total pressure of 50 ± 1.5 psia and stagnation temperature of 520 ± 15°R were chosen as the test conditions. These correspond to a Reynolds number per foot of 11.55×10^6 at the beginning of the test section. All recorded pressures and temperatures were non-dimensionalized by their respective stagnation conditions at the instant each measurement was taken. Run times were on the order of 15 sec.

Flow Configuration

In order to avoid wall curvature effects, the pressure gradients were generated along the flat wall of the test section by sting mounting compression surfaces along the tunnel center line as shown in Fig. 1. In addition, the leading edge of each ramp was attached to a thin plate which extended through the nozzle in order to eliminate any leading edge disturbances. The boundary-layer studied was, therefore, the one developed naturally along the flat wall of the test section and the fixed initial conditions were those generated at the end of the tunnel nozzle.

Model

The three compression surfaces, which spanned the width of the tunnel, were designed to isentropically compress the flow along the wall of the test section in a prespecified manner

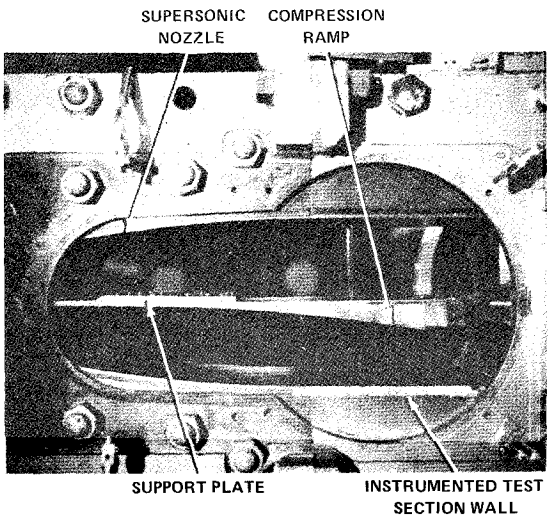

Fig. 1 Model installed in wind tunnel.

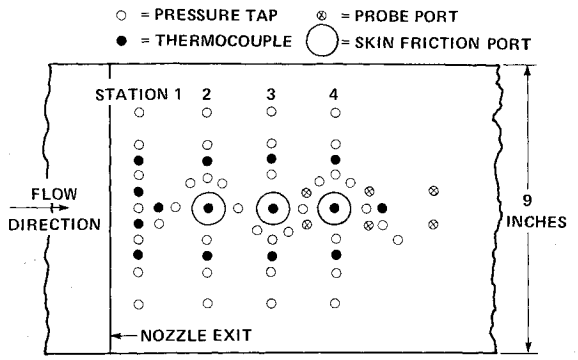

Fig. 2 Instrumented test section wall.

by a method of characteristics program. No adjustment of the ramp contours was made for boundary-layer growth. They were positioned so that the pressure gradients imposed on the test section wall would start approximately 1.5 in. downstream of the nozzle exit.

The wall of the test section was made of polished 304 stainless steel and instrumented with static pressure taps and thermocouples in both the lateral and axial direction. The static pressure taps were 0.031 in. in diameter and the thermocouples 0.010-in. copper-constantan wires press-fitted on the plate's surface. The location of these and their relative position to the nozzle exit is shown in Fig. 2. Also included in this figure are the locations of the four stations where the boundary-layer measurements were taken.

In order to probe the boundary layer, a traversing mechanism was built which attached to the bottom of the test section wall. It consisted of a 1-rpm motor which moved a rack gear on which the probes could be mounted. Ports were provided in the test section wall through which the probe could be inserted and attached to the traversing mechanism. These were located 0.5-in. off the wall centerline and were sufficiently far back so as not to interfere with measurements being taken at a given axial station as shown in Fig. 2. A 3-turn precision linear potentiometer was connected to the motor to determine the position of the probes at any given time. Traversing times of the boundary layer were on the order of 5–6 sec.

Instrumentation

All pressures were read using strain gauge transducers which were read on strip chart recorders with microvolt sensitivity. Wall pressures were read through a scani-valve arrangement at 0.25-sec intervals.

Temperatures were measured using copper-constantan thermocouples and read out on strip recorders which had electric cold junctions and indicated temperatures directly in °F.

Hot wire measurements were taken using the DISA Type 55D01 constant temperature anemometer and the DISA Type 55D35 RMS voltmeter using an integration time of 0.1 sec. The outputs of these were read on the strip recorders. One μsec spark schlieren and shadowgraph photographs were used to visually document the flow.

Probes

Four types of probes were used to document the boundary layer. These included pitot, cone static, total temperature and hot wire probes.

The response times of these probes were determined by positioning each probe at several fixed vertical positions in the boundary layer and recording their vertical position and output and then comparing these output readings with those obtained while traversing the layer for the same vertical positions. In all cases, it was found that the response time of each probe was undetectable within the limits of the experimental error incurred.

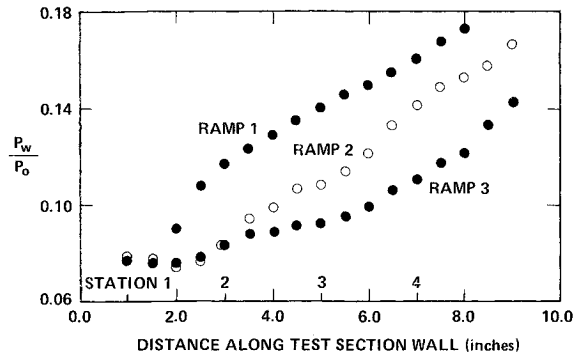

Fig. 3 Wall static pressure distribution.

The pitot probe was made by flattening 0.125-in.-o.d. stainless steel circular tubing to a rectangular cross section at the tip. The probe opening was 0.010 × 0.025 in. with the lip thickness being approximately 0.008 in.

The cone static probe was a 10° half angle brass cone with a base diameter of 0.062 in. The tip was precision ground to a sharp point. Four 0.013-in. ports were drilled perpendicular to the cone's surface approximately three quarters of the way back from the tip at 90° intervals around the circumference. The four ports led to a common chamber so that recorded pressures were the average pressures of the four ports. The accuracy and sensitivity to angle of attack of the cone static probe was established by direct calibration in the wind tunnel.

The total temperature probe was of the diffusor type and consisted of a 0.062-o.d., 0.038-i.d. in. stainless-steel tube with an insulated 0.005-in. copper-constantan thermocouple located approximately 0.100 in. back from the tube opening. Two vent holes were provided approximately 0.085 in. back from the tip to allow the gas to escape before it could be cooled by the tube's surface. The recovery factor was obtained by direct calibration for the Mach number range of 2.36 to 1.95 and the rest extrapolated from the data given in Ref. 8.

A DISA type 55F31 probe with a 5μm Pt-plated tungsten wire and an l/d of 250 was used for mean mass flow and turbulence intensity measurements. Four over-heat ratios were used.

Skin-Friction Balance

The skin-friction balance used in these experiments was a copy of that developed at the Naval Ordnance Lab. This device is described in detail in Ref. 9. Essentially the balance was used in the non-nulling mode in that deflections due to shear forces on the floating head were measured directly from the output of a linear variable differential transformer located inside the balance. This output was then compared to calibrations taken before and after each run. The area of the floating head was 0.496 in.^{2}. The head itself was constructed in an oblong shape (~0.5-in. axial × 1.0-in. lateral) so as to minimize the axial distance (and therefore pressure gradient) over which the measurements were made.

Data Reduction

In addition to the pitot, cone static, hot wire, and total temperature profiles measured at each station for each ramp, static temperature and pressure, velocity, density and mean mass flow profile were calculated at each using the measured profiles, the perfect gas relations, the Rayleigh pitot formula and the Mach number correlation given in Ref. 10. Since this correlation is good for supersonic flow only, Mach number profiles were incomplete near the wall. However, this was easily overcome by using the known pitot profile and assuming a static pressure profile between the last calculated point and the known wall value at each station. Mean mass flow profiles measured with the hot wire at stations 1 and 4 were obtained using the data of Laufer and McClellan,[11] and Kóvasznay and Törnmark.[12] Hot wire results for turbulence intensities at these same stations were obtained using the method described by Kistler[13] and Morkovin.[14] Because of the complexity of describing the method, it is recommended that the reader study the description provided in Refs. 13 and 14.

Errors in the measured and calculated profiles and skin friction data have been estimated and are given in Ref. 4 along with a more detailed description of the apparatus.

Experimental Results and Discussion

Flow Structure

The streamwise wall pressure distributions generated by the three ramps along the test section wall are shown in Fig. 3. It is seen that they do represent a systematic variation of both the magnitude and character of the pressure gradient in that ramp 1 generates a rather strong pressure rise with $d/dX(dP/dX) < 0$; ramp 2 generates a less severe pressure rise with $d/dX(dP/dX) \cong 0$; and ramp 3 generates a rather mild pressure rise with $d/dX(dP/dX) > 0$. In some instances, local slopes do not match those given above due to difficulties in machining the ramps, but the over-all character of each pressure gradient does.

The two-dimensionality of the flow was determined from the spanwise wall static pressure distributions taken at each of the four probing stations for each ramp. These measurements established that a substantial portion of the flow over the plate was two-dimensional in that the lateral pressure gradient at each station was extremely small when compared to the streamwise pressure gradient. Lateral pressure variations were less than 1% of the centerline pressure within ±2 in. of the centerline for all stations and ramps.

Figure 4 presents 1 μsec spark schlieren photographs of the flow over the test section wall generated by the three ramps. The turbid structure within the boundary layer and irregular outer edge, characteristic of turbulent viscous flows, is clearly evident. The disturbance in the lower left-hand corner is generated by a small step (~0.003 in.) at the intersection of the nozzle and test section. However, this disturbance is weak and does not adversely affect the flowfield except possibly by introducing some nonequilibrium effects into the boundary layer. The diagonal waves moving from the top left are compression waves generated by the ramps mounted in the center of the test section. The initial boundary-layer thickness and displacement thickness are approximately 0.37 and 0.095 in., respectively.

Results from the wall temperature measurements indicated that the wall was very nearly adiabatic in that the ratio $(T_w - T_{aw})/T_{aw}$ ranged between 0.051 and 0.035 for all three ramps.

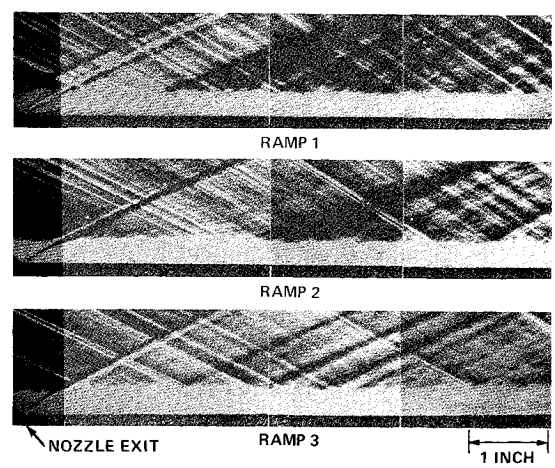

Fig. 4 One μsec Spark schieren photographs of wall boundary layer (flow is from left to right).

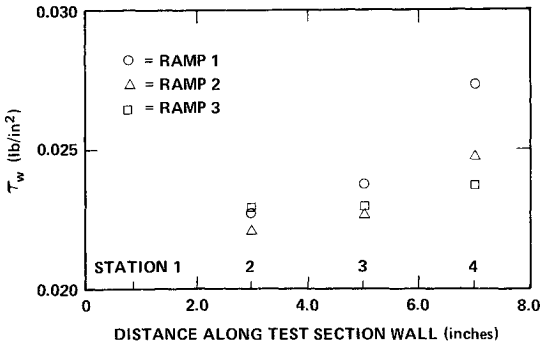

Fig. 5 Measured wall shear stress.

These were computed assuming a turbulent recovery factor of 0.89. It is therefore felt that any effects due to heat transfer in the data will be negligible.

Wall Shear

Direct measurements of wall shear taken with the skin friction balance are shown in Fig. 5 where four runs were made at each station and averaged. It is seen that the wall shear increases with axial distance in the adverse pressure gradient region. In addition, these increases are apparently a function of both the magnitude and character of the pressure gradient. For example, if the increase in wall shear at station 2 were strictly a function of the magnitude ($\Delta P/L$) of the pressure gradient, then one would expect the wall shear at this station for ramp 1 to be significantly higher than those of ramps 2 and 3 since its magnitude is appreciably higher (see Fig. 3). On the other hand, if the wall shear were strictly a function of the character (local dP/dX vs X) of the pressure gradient, then one would again expect the wall shear for ramp 1 at this station to be noticeably different than those of ramps 2 and 3 since its character is appreciably different from the others. However, neither of these hypotheses is valid as seen by the measurements shown in Fig. 5. Therefore, the measured increases in wall shear must be functions of both the magnitude and character of the pressure gradient.

Although it has been shown that the increases in wall shear are functions of both the magnitude and character of the pressure gradient, no attempt has been made to establish this relationship. It is felt that more data are needed before a relationship of this type can be established and it is therefore recommended that more research be conducted in this area.

Boundary-Layer Profiles

Since the purpose of this paper is to document what effects varying both the character and magnitude of an adverse pressure gradient will have on a supersonic turbulent boundary layer, it is paramount that the initial conditions be the same for all cases tested. In this respect, profiles were taken at the initial station (station 1) for each ramp and the resulting profiles agree with one another quite well. Those differences which do occur ($\pm 1\%$) are due to small variations in the disturbance created at the junction of the nozzle and test section wall (see Fig. 4) and experimental error.

The measured pitot pressure profiles for each ramp are shown in Fig. 6. It is seen that for each ramp, the local profile slope within the boundary layer increases with axial distance, at least for the outer 95% of the boundary layer where profile measurements were taken. In addition, when the three ramps are compared, differences in slope at a given station seemingly correspond to the magnitude of the pressure gradient at that station. For example, at station 3, the local pitot pressure slope for ramp 1, which has the largest magnitude of the three ramps, is the greatest, while those for ramps 2 and 3 are progressively smaller due to the smaller magnitudes of their respective pressure gradients. However, this is to be expected since the larger the magnitude of the pressure gradient, the lower the Mach number and thus, for the same total pressure, the higher the pitot pressure and greater the slope. Also, because of the way in which these pressure gradients were generated, the pitot pressure continues to increase with vertical distance outside the boundary layer, although at a much slower rate than observed within it, since there is an inviscid variation in the flow normal to the wall outside the layer. One might not expect this for the initial station since it is supposedly in a constant pressure region. However, due to the disturbance generated by the union of the nozzle and test section and its close proximity to the start of the pressure gradient, small variations in the free-stream properties are bound to occur. Finally, a definite decrease in the thickness of the boundary layer can be seen for ramp 1 with this decrease becoming progressively less for ramps 2 and 3. This is apparently due to compression of the boundary layer by the external pressure gradient and has been previously observed[6] on a concave compression surface.

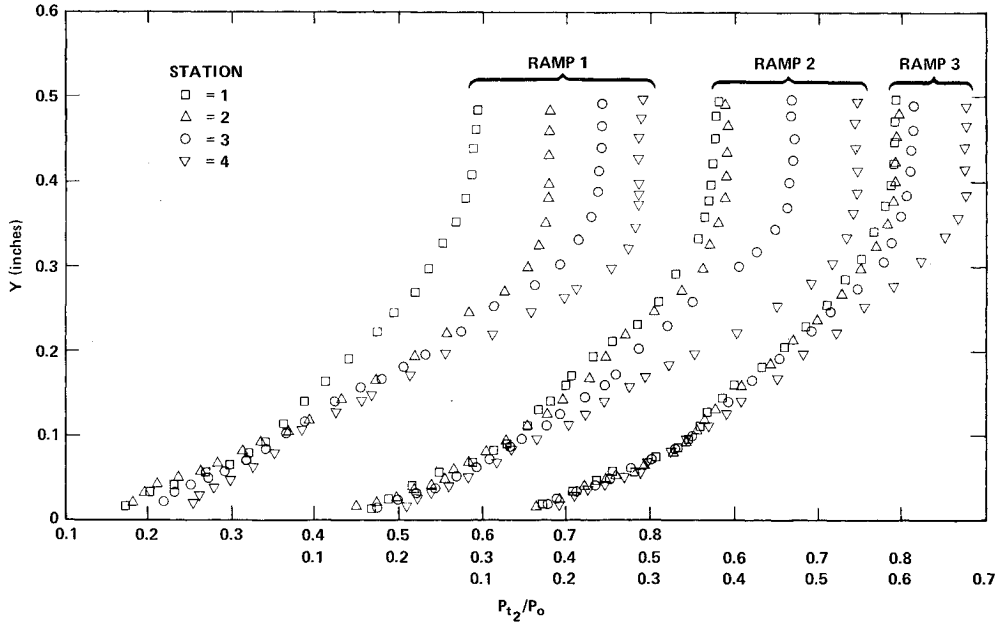

Fig. 6 Pitot pressure profiles.

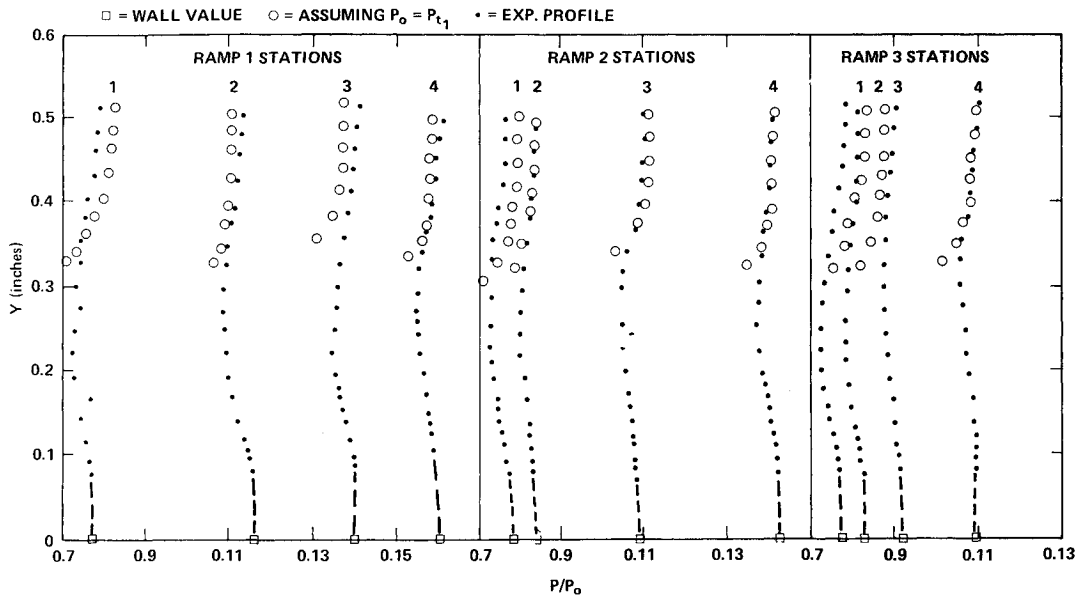

Fig. 7 Static pressure profiles.

The computed static pressure profiles are shown in Fig. 7. It is seen that the static pressure initially decreases with distance from the wall up to about two thirds of the boundary-layer thickness and then increases continuously through the rest of the layer for all stations and ramps. On the average, these pressure "deficits" decrease with axial distance in the adverse pressure gradient region. Since this bulge is most pronounced at the initial station, it is felt that it is due to the upstream favorable pressure gradient history of the boundary layer. Subjecting this profile to an adverse pressure gradient seems to decrease the static pressure bulge. Once outside of the boundary layer, the pressure continues to rise as the Mach number in the freestream decreases. Also shown on these plots are the pressures one would obtain in the outer portion of the layer assuming $P_o = P_{t_1}$, where P_{t_1} would be the total pressure of the flow at that point if it were isentropic. Although the flow just outside the boundary layer is not exactly isentropic, these results illustrate that it is very nearly so and that the disturbance generated at the union of the nozzle and test section walls is weak. Finally, the dashed lines in the figures represent the assumed static pressures that were used to compute Mach numbers less than 1.2.

The measured total temperature and computed static temperature profiles are shown in Fig. 8. The total temperature profiles indicate that the total temperature through the layer is nearly constant at all stations for all three ramps. However, near the wall, there is approximately a 1% decrease in the total temperature, due to viscous dissipation and a small amount of heat transfer. Also, about one quarter of the boundary-layer thickness from the wall, all profiles exhibit a total temperature overshoot which is characteristic of adiabatic, compressible boundary-layer flows. These overshoots maximize at about three quarters of the boundary-layer thickness and then decrease to the freestream value at the edge of the boundary layer. In addition, the adverse pressure gradients do not seem to affect the magnitude of these overshoots, at least within the accuracy of the experimental measurements.

Whereas the total temperature profiles are unaffected by the adverse pressure gradient, the static temperature profiles are in that the slopes associated with each ramp decrease with the magnitude of the pressure gradient. However, these differences are due to the change in velocity which accompanies the adverse pressure gradient and not some other flow phenomena.

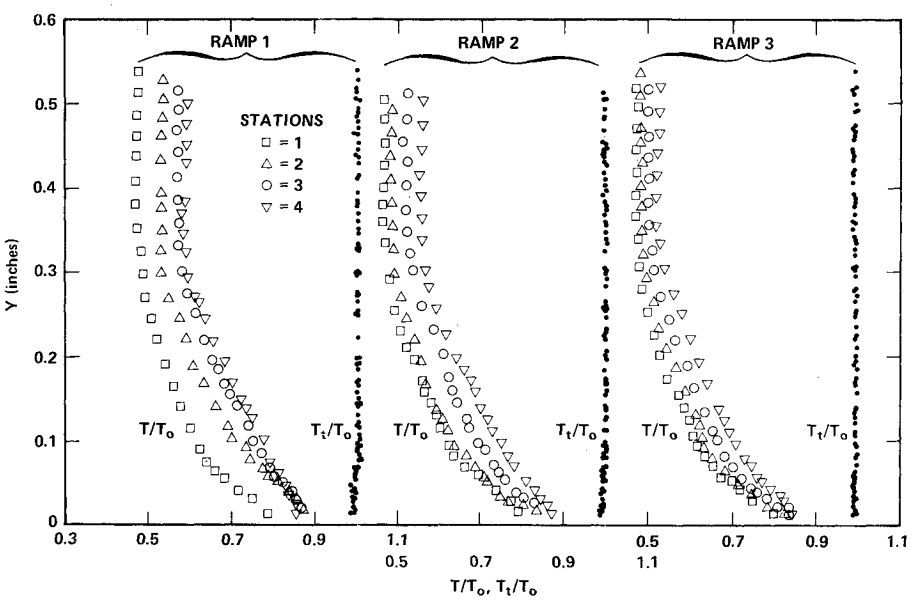

Fig. 8 Temperature profiles.

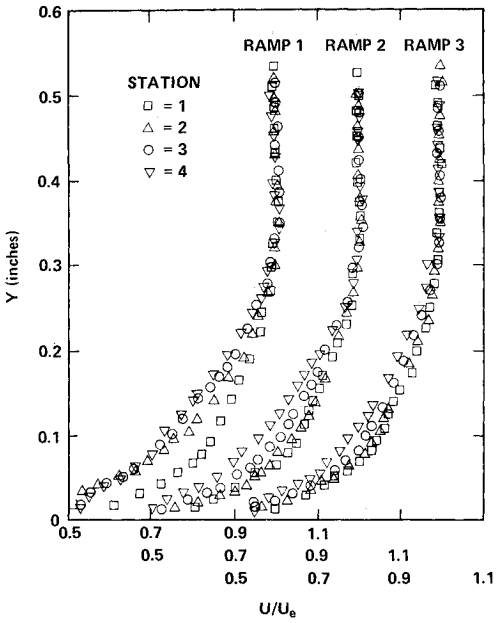

Fig. 9 Velocity profiles.

Also, the three static temperature profiles in the adverse pressure gradient region of ramp 1 converge near the wall, whereas those for ramps 2 and 3 do not.

The velocity profiles for each ramp, shown in Fig. 9, indicate a decrease in slope with distance in the adverse pressure gradient region. Again, this decrease seems to be a function of the magnitude of the pressure gradient. However, this is not true at the wall since the results of the skin-friction balance show increases in wall shear with axial distance, with these increases being most pronounced for the most severe pressure rises. As a consequence of this, one would expect the wall velocity gradient to increase with axial distance for each ramp. For this to occur the velocity gradient at station 4 for ramp 1 would have to decrease sharply in a region near the wall and then rapidly increase at the wall. This phenomena would also have to occur for stations 3 and 2 and ramps 2 and 3, but at progressively slower rates. The beginning of these sharp decreases can be seen in the velocity profiles for each ramp with the amount of this decrease increasing from station 2 through 4. This would also

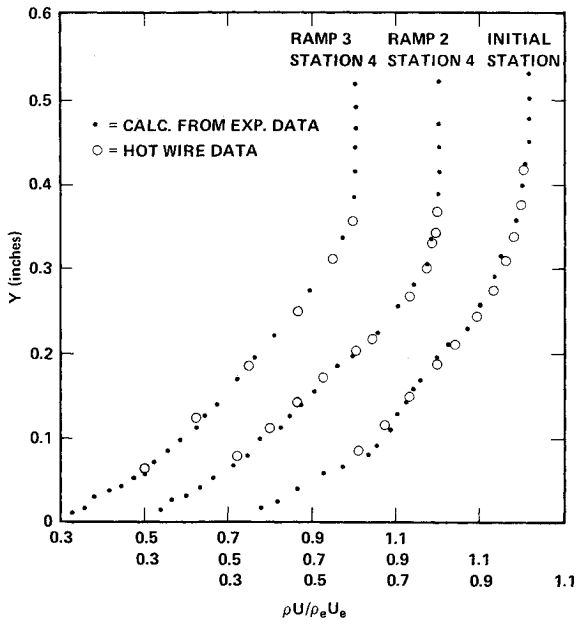

Fig. 10 Mass flow profiles.

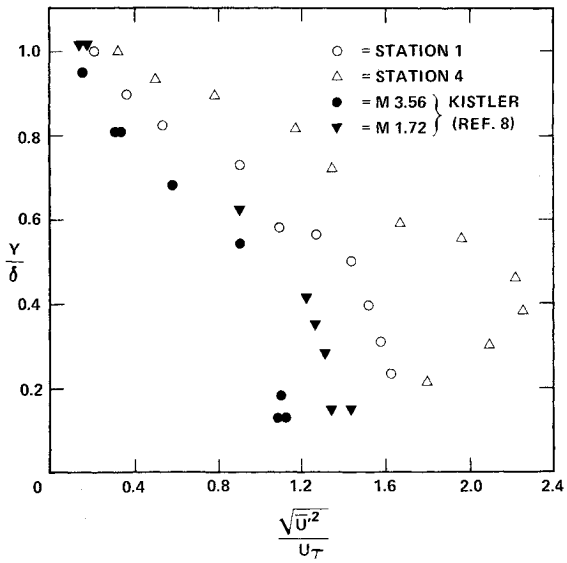

Fig. 11 Turbulence intensity profiles.

explain why the velocity, temperature, etc. profiles in the adverse pressure gradient region of ramp 1 converge near the wall, while those for ramps 2 and 3 do not, i.e., since the increases in wall shear are most pronounced for ramp 1 and the velocity gradient decreases with axial distance except at the wall, then the velocity profiles must cross (and therefore converge) at some nominal distance above the wall in order for the wall shear to increase. For ramp 1, this occurs within the measurement field. This must also occur for ramps 2 and 3, but not at as great a distance from the wall and therefore occurs between the last measured point and the wall and is not seen on the profile plots.

The mean mass flow profiles taken with the hot wire are shown in Fig. 10. Included on these plots are the mean mass flow profiles computed from the pitot, cone static, and total temperature surveys. Although there is a slight overshoot of the hot wire data when compared to the other in the outer portion of the boundary layer and an undershoot near the wall, these are to be expected as this trend has been observed before. In any event, both sets of data agree very well within the estimated experimental error (5.5%) and establish a set of redundant points which should dispel any doubts about the over-all accuracy of the data.

The turbulence intensities measured at stations 1 and 4 of ramp 2 are shown in Fig. 11. Because of the scatter in the data, it is estimated that the error of these results could be as much as $\pm 20\%$. However, they do indicate the trend of the turbulence intensities in that at the initial station, the intensity monotonically decreases with distance from the wall and exhibits a definite low freestream value. For station 4, which lies well within the adverse pressure gradient, the intensity increases with vertical distance from the wall, reaches a peak in the middle of the boundary layer, and then decreases to a relatively low freestream value. These trends were also observed by Sturek and Danberg.[6] The importance of the turbulence intensity in determining the empirical constant in an eddy viscosity (or Reynold's stress) model has previously been demonstrated by Schetz,[15] at least for turbulent wakes, where the constant was shown to be proportional to the intensity. One would expect this same trend to be valid for turbulent boundary-layer flows along walls, at least for the outer eddy viscosity model, and, assuming this to be the case, the current data would dictate that different values of the constant be used in the zero and adverse pressure gradient regions. However, more data is needed before any conclusive statement of this type can be made.

Figure 11 also includes the results of Kistler[13] for the zero pressure gradient case. It is seen that his intensities are somewhat lower than those measured at the initial station for this

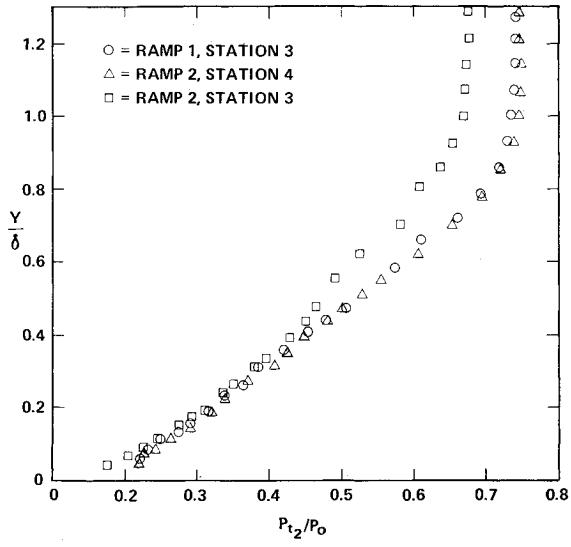

Fig. 12 Effect of pressure gradient magnitude on pitot profiles.

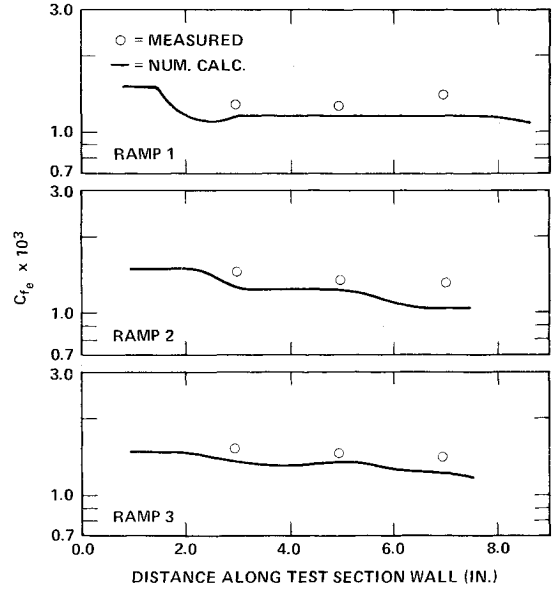

Fig. 14 Comparison of measured and computed wall shear stress.

set of experiments. However, for similar boundary layers the intensities are proportional to U/δ so that a thinner boundary layer would exhibit larger intensities than a thicker one. This would seem to be the case for the data shown, since the boundary-layer thickness in Kistler's experiments was 2–3 times as great as the present one. However, the boundary-layer reported in Ref. 13 was in equilibrium, whereas the present one was not due to the nozzle expansion and disturbance generated just upstream of the measuring station. It would, therefore, seem that the observed differences are due to a combination of the aforementioned effects and not any single one.

It has been stated all along that the profile shapes of each ramp seem to be a function of the magnitude of the adverse pressure gradient rather than its character, except, possibly, close to the wall. A conclusive demonstration of this is presented in Fig. 12 where the pitot profiles of ramp 1, station 3 and ramp 2, stations 3 and 4 have been plotted. Station 3 of ramp 1 and station 4 of ramp 2 were chosen for comparison because they both have about the same static pressure rise ($\Delta P/P_o = 0.0626$ and 0.0636, respectively) while station 3 of ramp 2 was chosen because its static pressure rise ($\Delta P/P_0 = 0.0303$) is significantly different than those previously noted. It is seen that for approximately the same static pressure rise (and therefore magnitude), the measured pitot profiles are almost exactly the same, with any difference being attributable to the small difference in pressure gradient magnitude between the two, while the pitot profile associated with the less severe magnitude is quite different both in its slope and numerical value. Further details of the experimental data are given in Ref. 4.

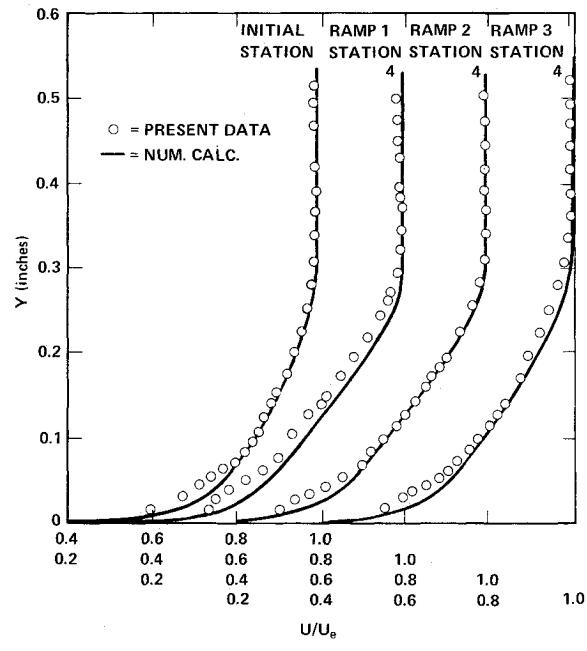

Fig. 13 Comparison of experimental and analytical velocity profiles.

Comparison of Experiments with Numerical Calculations

As stated previously, the experimental results contained herein are compared with numerical calculations based on the work of Miner, Anderson, and Lewis.[7] Briefly, this program solves the turbulent boundary-layer equations using a Crank-Nicolson type implicit finite difference scheme with the equations transformed into a Levy-Lees coordinate system. A two-layer eddy viscosity model is used with the inner law based on Van Driest's model and the outer law based on Clauser's model. The program is started at the beginning of the tunnel nozzle assuming the following initial profiles

$$U/U_e = 1 - e^{-\eta} \tag{1}$$

$$h/h_e = h_w/h_o + [1-(h_w/h_o)]U/U_e \tag{2}$$

where η = transformed normal coordinate. The wall pressure distributions shown in Fig. 3 are the only experimental inputs and are assumed to be the pressures at the edge of the boundary layer. In addition, the turbulent boundary-layer equations are assumed valid throughout the entire nozzle and test section even though some initial portions of the nozzle may be laminar. Only one modification to the published version of the program was necessary in order to run the adverse pressure gradient cases. This involved distinguishing edge velocities in the expansion portion of the nozzle from those created along the test section wall due to the compression ramps which, in some cases, were the same. If more information is desired by the reader about this program and the governing equations, it is recommended that he read Refs. 7, 16, and 17.

The results of the numerical calculations are shown in Figs. 13 and 14 where velocity and skin-friction predictions have been chosen for comparison. Also, only the initial and final station profiles are compared, as it is felt that these will best represent the accuracy of the numerical scheme.

For the velocity profiles (Fig. 13), the numerical calculations predict a somewhat fuller velocity profile than those measured,

especially in the region near the wall, with the over-all prediction being fairly good at the initial station and final stations of ramps 2 and 3. The maximum deviation between the predicted and measured values for these three stations is 10% in the region near the wall. For ramp 1, station 4, the numerical calculations consistently overpredict the magnitude of the velocity profile. However, this is the last station in the most severe adverse pressure gradient and if any deviations between predicted and actual profiles were to occur, one would expect them to materialize at this station.

The comparisons of predicted and measured skin friction are shown in Fig. 14 for all three ramps where the measured values of the wall shear were nondimensionalized by the same values of the dynamic pressure as those in the numerical calculations so that any differences in the measured and predicted edge conditions would not affect these comparisons. It is seen that the predicted values are about 8–10% lower than those measured at station 2 for all three ramps with this difference generally increasing with axial distance in the adverse pressure gradient. It is also seen that, on the average, the more severe the pressure gradient, the worse the predictions become at each of the measuring stations. Differences at the final station are as much as 20%.

On the basis of these comparisons, it is felt that the numerical scheme tested, and others like it, are amenable for engineering calculation of flows of the type studied herein, since reasonable accuracy between predicted and measured quantities has been demonstrated. However, it becomes increasingly suspect with severity of the adverse pressure gradient, and should, therefore, be compared to data generated in a more severe pressure gradient to assure its validity in this regime.

Conclusions and Recommendations

An accurate set of experimental data have been presented for a supersonic turbulent boundary layer subjected to a systematic variation of three (3) adverse pressure gradients starting with the same initial conditions. Sufficient measurements have been taken to completely define or permit calculation of all important flow characteristics. Analysis of the experimental data has led to the following conclusions; 1) Profile shapes are affected more by the magnitude of the pressure gradient than its character except, possibly, in a region very close to the wall. 2) Subjecting an adiabatic supersonic turbulent boundary layer to an adverse pressure gradient increases the wall shear, with this increase being a function of both the magnitude and character of the pressure gradient. No relationship between these is established because of insufficient data. It is recommended that more experiments be conducted in this area. 3) The total temperature overshoot, characteristic of adiabatic compressible boundary layers, does not seem to be affected by the adverse pressure gradient. 4) The profile of the turbulence intensity exhibits a maximum in the middle of the boundary layer in the adverse pressure gradient region, whereas the one at the initial station decreases monotonically outward from the measurement position closest to the wall. Both exhibit low intensities at the edge of the boundary layer. 5) Comparison of the experimental results with a numerical solution indicates that the numerical solution predicts profiles fairly well except for the last station of the most severe pressure gradient. However, measured values of the skin friction are between 8 and 20% higher than those predicted with the difference increasing with axial distance in the adverse pressure gradient and with the difference being most pronounced for the most severe pressure gradient.

References

[1] Kline, S. J., Sorran, G., Morkovin, M. V., and Cockrell D. J., eds., *Proceedings, Computation of Turbulent Boundary Layers—1968, AFOSR-IFP-Stanford Conference, Vol. 1*, 1968.

[2] Coles, D. E. and Hirst, E. A., eds., *Proceedings, Computation of Turbulent Boundary Layers—1968, AFOSR-IFP-Stanford Conference, Vol. 2*, 1968.

[3] Bertram, M., *Compressible Turbulent Boundary Layers*, NASA SP-216, Dec. 1968.

[4] Waltrup, P. J. and Schetz, J. A., "An Experimental Investigation of a Compressible Turbulent Boundary Layer Subjected to a Systemat Variation of Adverse Pressure Gradients," VPI-E-71-18, Aug. 1971, Virginia Polytechnic Inst. and State Univ., Blacksburg, Va.

[5] Voisinet, R. L. P., Lee, R. E., and Yanta, W. J., "An Experimental Study of the Compressible Turbulent Boundary Layer with an Adverse Pressure Gradient," *AGARD Conference Proceedings, No. 93 on Turbulent Shear Flows*, Sept. 1971.

[6] Sturek, W. B. and Danberg, J. E., "Supersonic Turbulent Boundary Layer in Adverse Pressure Gradient Part I: The Experiment," *AIAA Journal*, Vol. 10, No. 4, April 1972, pp. 475–481; also "Part II: Data Analysis," *AIAA Journal*, Vol. 10, No. 5, May 1972, pp. 630–636.

[7] Miner, E. W., Anderson, E. C., and Lewis, C. H., "A Computer Program for Two-Dimensional and Axisymmetric Nonreacting Perfect Gas and Equilibrium Chemically Reacting Laminar, Transitional, and-or Turbulent Boundary Layer Flows," Rept. VPI-E-71-8, May 1971, Virginia Polytecnic Inst. and State Univ., Blacksburg, Va.

[8] Hottel, H. C. and Kalitinsky, A., "Temperature Measurements in High Velocity Air Streams," *Journal of Applied Mechanics*, March 1945.

[9] Bruno, J. R., Yanta, W. J., and Richer, D. B., "Balance for Measuring Skin Friction in the Presence of Heat Transfer," NOLTR-69-56, June 1969, Naval Ordnance Lab., White Oak, Md.

[10] Volluz, R. J., *Handbook of Supersonic Aerodynamics* Section 20, *Wind Tunnel Instrumentation and Operation*, NAVORD Rept. 1488, Vol. 6, Jan. 1961, Naval Ordnance Lab.

[11] Laufer, J. and McClellan, R., "Measurements of Heat Transfer from Fine Wires in Supersonic Flow," *Journal of Fluid Mechanics*, Vol. 1, Pt. 3, Sept. 1956.

[12] Kóvasznay, L. and Törnmark, S., "Heat Loss of Hot-Wires in Supersonic Flow," Bumblebee Report 127, 1950.

[13] Kistler, A. L., "Fluctuating Measurements in Supersonic Turbulent Boundary Layers," BRL Rept. 1052, Aug. 1958, Ballistic Research Lab., Aberdeen, Md.

[14] Morkovin, M. V., "Fluctuations and Hot-Wire Anemometry Compressible Flows," AGARDograph 24, Nov. 1956.

[15] Schetz, J. A., "Some Studies of the Turbulent Wake Problem," *Astronautics Acta*, Vol. 16, 1971, pp. 107–117.

[16] Lewis, C. H., Anderson, E. C., and Miner, E. W., "Nonreacting and Equilibrium Chemically Reacting Turbulent Boundary-Layer Flows," AIAA Paper 71-597, Palo Alto, Calif., 1971.

[17] Anderson, E. C. and Lewis, C. H., "Laminar or Turbulent Boundary-Layer Flows of Perfect Gases or Reacting Gas Mixtures in Chemical Equilibrium," CR-1893, Oct. 1971, NASA.